Focal aggregation of voltage-gated, Kv2.1 subunit-containing, potassium channels at synaptic sites in rat spinal motoneurones

Elizabeth A. L. Muennich and R. E. W. Fyffe

Department of Anatomy and Physiology, Wright State University, Dayton, OH 45435, USA

Delayed rectifier K^+ currents are involved in the control of α-motoneurone excitability, but the precise spatial distribution and organization of the membrane ion channels that contribute to these currents have not been defined. Voltage-activated Kv2.1 channels have properties commensurate with a contribution to delayed rectifier currents and are expressed in neurones throughout the mammalian central nervous system. A specific antibody against Kv2.1 channel subunits was used to determine the surface distribution and clustering of Kv2.1 subunit-containing channels in the cell membrane of α-motoneurones and other spinal cord neurones. In α-motoneurones, Kv2.1 immunoreactivity (-IR) was abundant in the surface membrane of the soma and large proximal dendrites, and was present also in smaller diameter distal dendrites. Plasma membrane-associated Kv2.1-IR in α-motoneurones was distributed in a mosaic of small irregularly shaped, and large disc-like, clusters. However, only small to medium clusters of Kv2.1-IR were observed in spinal interneurones and projection neurones, and some interneurones, including Renshaw cells, lacked demonstrable Kv2.1-IR. In α-motoneurones, dual immunostaining procedures revealed that the prominent disc-like domains of Kv2.1-IR are invariably apposed to presynaptic cholinergic C-terminals. Further, Kv2.1-IR colocalizes with immunoreactivity against postsynaptic muscarinic (m2) receptors at these locations. Ultrastructural examination confirmed the postsynaptic localization of Kv2.1-IR at C-terminal synapses, and revealed clusters of Kv2.1-IR at a majority of S-type, presumed excitatory, synapses. Kv2.1-IR in α-motoneurones is not directly associated with presumed inhibitory (F-type) synapses, nor is it present in presynaptic structures apposed to the motoneurone. Occasionally, small patches of extrasynaptic Kv2.1-IR labelling were observed in surface membrane apposed by glial processes. Voltage-gated potassium channels responsible for the delayed rectifier current, including Kv2.1, are usually assigned roles in the repolarization of the action potential. However, the strategic localization of Kv2.1 subunit-containing channels at specific postsynaptic sites suggests that this family of voltage-activated K^+ channels may have additional roles and/or regulatory components.

(Received 30 September 2003; accepted after revision 5 November 2003; first published online 7 November 2003)
Corresponding author R. E. W. Fyffe: Department of Anatomy and Physiology, Wright State University, Dayton, OH 45435, USA. Email: robert.fyffe@wright.edu

A wide variety of ionic currents underlie the excitability and firing patterns of α-motoneurones in the mammalian spinal cord (McLarnon, 1995; Kiehn & Eken, 1998; Kiehn *et al.* 2000; Rekling *et al.* 2000; Powers & Binder, 2001). Studies of macroscopic (Takahashi, 1990) and single channel (Safronov *et al.* 1996) membrane currents in α-motoneurones have revealed the presence and functional characteristics of multiple types of voltage-gated K^+ currents, including outwardly directed transient (A-type; I_A) and delayed rectifier (I_K) currents. The expression of these currents is developmentally regulated (Gao & Ziskind-Conhaim, 1998; Ribera, 1999), but the precise pattern of expression and localization of the underlying voltage-gated K^+ channels in α-motoneurones is not known.

Several lines of evidence suggest that channels formed by Kv2.1 subunits (members of the voltage-gated *Shab* family) are major contributors to delayed rectifier K^+ currents in vertebrate neurones (Murakoshi & Trimmer, 1999; Blaine & Ribera, 2001). Kv2.1 subunits may form

 DOI: 10.1113/jphysiol.2003.056192

heteromeric channels in association with modulatory α-subunits, or, with other subunits of the Kv2.1 subfamily (e.g. Kerschensteiner *et al.* 2003). Kv2.1 channel proteins have a unique C-terminal domain proximal restriction and clustering signal and are preferentially targeted to the soma and proximal dendrites of cultured hippocampal neurones and a variety of cortical principal cells and interneurones (Scannevin *et al.* 1996; Du *et al.* 1998; Lim *et al.* 2000; Antonucci *et al.* 2001). Since Kv2.1 subunits are expressed throughout the CNS, it is of interest to determine whether they exhibit similar polarized expression patterns in the soma and dendrites of spinal motoneurones and interneurones.

Single channel and ensemble I_A and I_K currents recorded from membrane patches on the soma and apical dendrites of hippocampal and cortical pyramidal neurones revealed key information about the density and distribution of voltage-gated K^+ channels in these central neurones (e.g. Hoffman *et al.* 1997; Bekkers, 2000*a*,*b*; Korngreen & Sakman, 2000; see also Storm, 2000). These studies demonstrate gradients of channel density along the dendrites, although there are specific differences in the precise organization of the channels in the two main cell types that were analysed (Storm, 2000). However, even in neurones that are amenable to direct patch recording, questions remain as to whether or not the recorded channels are present in synaptic and/or extrasynaptic membrane in the soma and dendrites.

Faced with the difficulty of obtaining comprehensive patch-clamp data from motoneurone dendrites *in situ*, channel localization using immunohistochemistry is a valuable step in understanding the role(s) of specific postsynaptic voltage-gated K^+ channels in motoneurones, and other spinal neurones. This approach, even though it cannot determine channel function, can provide direct evidence that addresses the critical question of whether or not the channels are present at synaptic or extrasynaptic sites in the postsynaptic membrane. Detailed ultrastructural analyses have previously revealed that approximately 50% of the somatic membrane area (and a slightly lower proportion of dendritic membrane) of α-motoneurones is associated with a structurally and functionally diverse set of presynaptic nerve terminals; the remaining, extrasynaptic, surface membrane is largely apposed by glial processes (e.g. Conradi *et al.* 1979; Kellerth *et al.* 1979; Rose & Neuber-Hess, 1991; Brännström, 1993; Starr & Wolpaw, 1994; Fyffe, 2001). A specific population of presynaptic terminals, the C-terminals (Conradi, 1969), form synapses exclusively on the soma and proximal dendrites of α-motoneurones, and although they are by no means the most numerous class of synapse their large size means that they contribute a significant proportion of the overall synaptic coverage at the soma (e.g. Fyffe, 2001). The synapses established by C-terminals are characterized by the presence of subsynaptic cisternae, and they have been demonstrated to be cholinergic in nature (Nagy *et al.* 1993; Li *et al.* 1995; Hellström *et al.* 1999; Wetts & Vaughn, 2001). In addition, these cholinergic C-terminals are associated with postsynaptic muscarinic m2-type receptors in spinal α-motoneurones (Skinner *et al.* 1999; Hellström *et al.* 2003).

In the present study, specific antibodies were used to define the membrane distribution of Kv2.1 channel subunits in α-motoneurones and interneurones in the rat spinal cord. Channel subunit expression and distribution were cell type specific; moreover, large clusters of Kv2.1 subunit-containing channels in α-motoneurones were primarily targeted to synaptic rather than to extrasynaptic membrane sites, and were found to associate particularly with cholinergic C-terminals on the soma and proximal dendrites. Preliminary data from this study have been published in abstracts (Muennich *et al.* 2002; Fyffe *et al.* 2002).

Methods

Immunohistochemistry

Adult male Sprague-Dawley rats were killed with an intraperitoneal overdose of sodium pentobarbital (>80 mg kg^{-1}). The animals were perfused transcardially with a 4°C vascular rinse (0.01 M phosphate buffer with 3.4 mM KCl, 137 mM NaCl, and 6 mM $NaHCO_3$, pH 7.3) followed by 4% paraformaldehyde in 0.1 M phosphate buffer (for electron microscopy, 0.25%–0.5% gluteraldehyde was added to the fixative). Spinal segments L4 and L5 were dissected into blocks and postfixed for 0, 2, or 4 h, and then immersed for 12–24 h in 0.1 M phosphate buffer (pH 7.4) with 15% sucrose, at 4°C. All procedures were performed according to National Institutes of Health guidelines and approved by the Wright State University Laboratory Animal Care and Use Committee.

Transverse sections of spinal cord were obtained from a freezing sliding microtome (at 50 μm section thickness) and placed into scintillation vials, or from a cryostat (at 20 μm thickness), in which case the sections were collected directly on to gelatin-coated slides. Following washing and blocking with normal horse serum (10%, in phosphate-buffered saline buffer (PBS-T; 0.01 M phosphate buffer, pH 7.2, with 0.88% NaCl, 0.02% KCl, and 0.1% Triton X-100), sections were incubated, for 2–4 h at room temperature or 24–48 h at 4°C, with primary antibodies (see below) diluted in PBS-T. The

following primary antibodies and dilutions were used, singly and/or in combination: mouse anti-Kv2.1 (Upstate Biotechnology, Lake Placid, NY, USA; 1 : 250), rabbit anti-m2 muscarinic receptor (Alomone, Jerusalem; 1 : 250), rabbit antisynaptophysin (Zymed, San Francisco, CA, USA; 1 : 500), goat antivesicular acetylcholine transporter (anti-VAChT, PharMingen, San Diego, CA, USA; 1 : 1000), rabbit anticalbindin (Swant, Bellinzona, Switzerland, 1 : 20 000), guinea pig anti-5-HT (gift from Dr J. C. Pearson, Wright State University, 1 : 5000), guinea pig antivesicular glutamate transporter 1 (anti-VGluT1; Chemicon, Temecula, CA, USA; 1 : 1000), mouse anti-gephyrin (mAb 7a; Boehringer Mannheim, Indianapolis IN, USA; 1 : 200), rabbit anti-choline acetyltransferase (anti-ChAT, Calbiochem, Darmstadt, Germany; 1 : 250). In addition, a second commercially available antibody against Kv2.1 was tried in some experiments (rabbit anti-Kv2.1, Alomone; 1 : 250). The two anti-Kv2.1 antibodies produced overlapping cell surface labelling patterns but since the Alomone polyclonal antibody also produced substantial cytoplasmic labelling, the monoclonal anti-Kv2.1 antibody obtained from Upstate was used for all analysis and illustrations in this work. The specificity of all the antibodies has been confirmed in our laboratory and elsewhere. In our laboratory, Western blotting of rat brain (at an antibody concentration of 1 μg ml^{-1}; detection with Phototope-Star Western Blot detection kit, New England Biolabs) revealed a single band around 110 kDa. For the anti-Kv2.1 antibody, staining was eliminated by preabsorption (1 μg : 1 μg) with a peptide corresponding to residues 837–853 of rat Kv2.1; these amino acid residues form the C-terminal end of the fusion protein used to generate the monoclonal antibody (see, e.g. Murakoshi & Trimmer, 1999). Further, no labelling is observed when the primary antibody is omitted from the process. In some experiments, spinal neurones and laminar boundaries were visualized with NeuroTrace green fluorescent Nissl stain (Molecular Probes, Inc, Eugene, OR, USA; 1 : 100). For immunofluorescence, immunoreactive sites were visualized with secondary antibodies (Jackson, West Grove, PA, USA) appropriate for the respective primary antibodies, namely, donkey-anti-mouse (1 : 50), donkey-anti-rabbit (1 : 50), and donkey-anti-goat (1 : 50) IgGs coupled to Cy3 or to fluorescein isothiocyanate (FITC); secondary antibodies were diluted in PBS-T, and the incubation time was 1.5 h. Sections that were processed free-floating in vials were then mounted onto gelatin-coated slides; all slides were cover-slipped with Vectashield (Vector, Burlingame CA, USA). Single and dual immunofluorescence was analysed on an Olympus Fluoview laser-scanning confocal microscope (argon 488/krypton 568 laser lines for excitation of FITC and Cy3, respectively). Emission light from the fluorochromes was separated using a dichroic mirror (EDM570) and emission filters with bandpass of 510–550 nm (FITC channel) and longpass of 585 nm (Cy3 channel). Optical sections were obtained through each cell at 0.5 μm separation in the Z-axis, using a $\times$100 oil immersion objective (NA 1.4) or $\times$60 dry objective (NA 0.9). Images captured with the $\times$100 objective were used for measurement of the area of '*en face*' clusters in single optical sections selected from each stack of serial optical sections. For selection and measurement of clusters within the '*en face*' area we used an automatic tracing procedure incorporating a threshold paradigm (selection of pixels at 33% of maximum fluorescence intensity, and rejection of clusters below 0.1 μm^2; see Fig. 1*B* and *C*). This produced results consistent with a manual tracing approach, and generated cluster dimensions that were similar to those measured with electron microscopy. Subsequent analysis used ImagePro Plus (version 4.1; Media Cybernetics) and all images were produced using CorelDRAW (version 11.0).

Pre-embedding immuno-electron microscopy

Glutaraldehyde-fixed Vibratome sections (50 μm thick) were treated with 1% $NaBH_4$ in PBS (Triton X-100 was omitted from all solutions for electron microscopy processing) for 30 min and then washed thoroughly with PBS. Sections were incubated with the monoclonal anti-Kv2.1 antibody (1 : 250) in PBS for 2–4 days at 4°C and then processed with ABC-peroxidase kits (Vector, Burlingame, CA, USA). Peroxidase histochemistry was developed with 0.02% diaminobenzidine (DAB, Sigma) and 0.01% H_2O_2 diluted in 0.05 M Tris buffer, pH 7.4, with an 8–10 min reaction time as above. In some experiments, silver enhancement of reaction product was performed. Sections were incubated an additional 20 min in 2.5% gluteraldehyde in 0.1 M PBS and washed 3 times with tris-maleic acid buffer, rinsed with nanopure H_2O and placed in silver nitrate solution for 10 min at 60°C. Following washing, the sections were placed in 0.05% gold chloride solution for 2 min at room temperature and again washed with nanopure H_2O. Unbound silver particles were removed by washing in 3.0% sodium thiosulphate (2 min), and additional washes in nanopure H_2O and 0.01 M PBS. Sections were postfixed for 40 min in 2% osmium tetroxide, stained with 1.0% uranyl acetate in 70% ethanol, and dehydrated in a graded series of ethanol followed by 2 $\times$ 5 min in propylene oxide. Processed

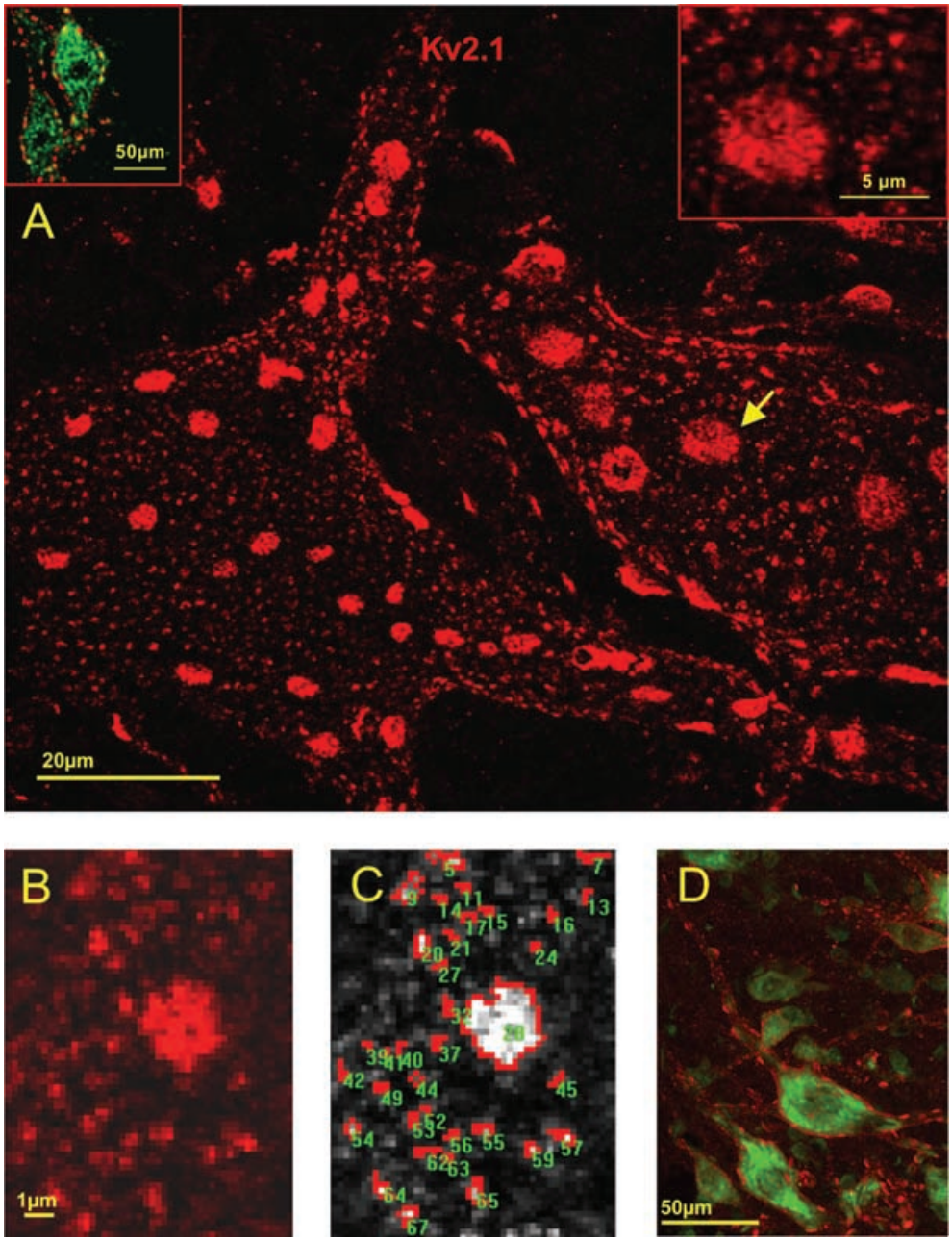

Figure 1.
The mosaic of Kv2.1 subunit-containing channel clusters in the plasma membrane of motoneurones. *A*, projected confocal image of Kv2.1-IR (red) in two adjacent motoneurones, demonstrating the range in size and complexity of Kv2.1 clusters. The image is a stack of 24 optical sections sampled at 0.5 μm intervals and superimposed to reveal the '*en face*' architecture of a 'hemi-neurone'. The inset at upper left is a single optical section to demonstrate Kv2.1-IR (red) surrounding motoneurones identified by ChAT-IR (green). The inset at upper right shows a higher magnification image of a region of surface membrane depicted (arrow) in the main part of the figure. The inset displays the fine structural detail of small and large disc-like clusters and demonstrates that they are formed by aggregates of small punctae. *B* and *C*, measurement of cluster area. *B* shows a screen image of a single optical section capturing an '*en face*' region of surface membrane, highly magnified (pixel size 0.16 μm). Kv2.1 immunofluorescence intensity is defined by grey scale in *C* (lighter shades more intense fluorescence). with highlighting (red) of the areas selected by the thresholding paradigm for measurement. Note again the complex structure and shape of the clusters. *D*, a low power image showing cross-sectioned motoneurones (Nissl; green) and Kv2.1-IR (red), demonstrating the extent of immunofluorescence on the dendrites, as well as the 'edge-on' visualization of large discs along the surface membrane.

sections were flat-embedded in Epon–Araldite between two Teflon-coated coverslips after overnight incubation in 1 : 1 propylene oxide/Epon–Araldite. Small areas containing immunolabelled motoneurones were selected from the section and glued to a resin block. Ultrathin sections were cut at 80 μm with a Sorvall MT 6000 ultramicrotome. Serial sections were collected on copper grids coated with a thin layer of Formvar, counterstained with uranyl acetate and lead citrate for 1 min, and viewed on a Philips EM201 transmission EM equipped with a Gatan digital camera. Digital images were used for synaptological survey of the neurone surface and the determination of synapse type and distribution of immunoreactivity. Electron micrographs incorporated in the figures in this paper were produced in CorelDRAW from standard electron microscopy negative plates that were scanned at 200 dpi.

Results

α-motoneurones were identified by their size and location (fluorescent Nissl staining), by the presence of ChAT-immunoreactivity (-IR; Fig. 1*A*, top left inset), or by the presence of numerous C-terminals (VAChT-IR) apposed to their somatic surface (e.g. Alvarez *et al.* 1999). Renshaw cells were identified by their calbindin-IR (Fig. 3*A*1; Carr *et al.* 1998) or characteristic gephyrin expression pattern (Alvarez *et al.* 1997), and by their location in ventral lamina VII.

Kv2.1 channel immunolabelling and organization in α-motoneurones

Kv2.1-IR in lamina IX clearly outlined, in punctate fashion, the soma and proximal dendrites of α-motoneurones (Fig. 1*D*). The pattern of staining around the perimeter of cross-sectioned somata, with little or no cytoplasmic Kv2.1-IR in the cell body, suggests that the patches of immunoreactivity are localized in the plasma membrane and most likely reflect the distribution of clusters of Kv2.1 channels in the surface membrane. In sections where motoneurone dendrites could be unequivocally traced distally within the plane of section, distinct Kv2.1-IR punctae were detected in dendritic membrane up to several hundred μm from the soma. In the surrounding neuropil, Kv2.1-IR also outlined the circumference of small diameter processes cut perpendicular to the plane of section. Most prominently, the membrane immunostaining observed around the perimeter of the soma is characterized by the presence of intensely labelled large patches of immunoreactivity, in addition to the more or less uniform distribution of discrete small punctae that are interspersed between these large patches (Fig. 1*A* and *C*).

Projected stacks of serial optical sections permitted immunoreactive areas to be viewed '*en face*' on the surface of the cell. These observations confirm that the prominent large patches viewed 'edge on' around the perimeter of the cell have extensive disc-like shapes, and are distributed throughout a relatively dense mosaic of smaller clusters (Fig. 1*A*). The small patches of immunoreactivity were of irregular shape, and some of the large discs had perforations in their interior. Many of the small patches, as well as the larger discs, appeared to be composed of aggregates of discrete spot-like punctae (e.g. Fig. 1*A*, top right inset).

Discrete clusters of immunoreactivity, whether they were comprised of a single spot, or contained a few, or many (i.e. in a large disc) individual punctae, were measured from magnified single optical sections of membrane imaged '*en face*' (e.g. Fig. 1*B* and *C*). The quantitative analysis of *en face* clusters ($n = 2673$; 26 cells from 4 rats) revealed a very broad distribution of cluster sizes (range 0.13–13.80 μm^2, mean = 1.14 μm^2; Fig. 2), heavily skewed to the left by the dominant subpopulation of small clusters (here arbitrarily defined as those less than 2.0 μm^2 in area; $n = 2326$, 87.0%). The remaining 347 (13.0%) clusters, including the large disc-shaped aggregates, when taken independently of the small clusters, had a mean area of 6.38 $\pm$ 2.63 μm^2.

The density of channel clusters in the somatic membrane was estimated from a sample of 1130 *en face* clusters (1062 small and 68 large) from selected areas of 13 motoneurones. In the measured areas (total sampled membrane 6330 μm^2), small clusters were present at a

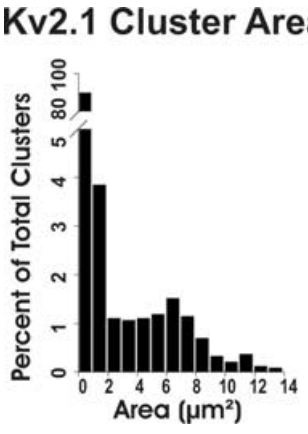

Figure 2.
Quantitative analysis of Kv2.1 subunit-containing channel clusters. The distribution of cluster areas ($n = 2673$) is highly skewed. Small clusters (area less than 2 μm^2) comprise 87% of the population.

frequency of about 17 clusters per 100 μm^2 of surface membrane. Large clusters are much less abundant, with about 1.0 cluster per 100 μm^2 of surface membrane.

Optical sectioning through the whole soma permitted an estimate of the number of large clusters present in the somatic membrane to be made. Analysis of 20 cells indicates that there are 36.5 ± 7.2 (mean ± S.D., $n = 730$) large clusters per motoneurone soma. The mean somatic surface area of rat motoneurones has been estimated to be approximately 3900 μm^2 (Chen & Wolpaw, 1994). Taking this surface area value, and the estimate of the number of disc-like clusters per cell (i.e. 36.5), we obtain an independent density estimate of approximately 1.07 large clusters per 100 μm^2. This is obviously in extremely close agreement with the density estimate derived above, suggesting that the areas sampled for measurement of cluster size and density are quite representative of the somatic membrane surface as a whole.

By definition, due to the punctate nature of the immunolabelling, there exists intervening membrane surrounding each cluster that appears devoid of channel labelling. However, it also appeared from the confocal reconstructions and *en face* images that each large disc might be surrounded by a distinct halo in which Kv2.1-IR is diminished or lacking (e.g. Fig. 1*A* and *B*). To explore this possibility, the distances (nearest edges) between small clusters, between large discs, and between large discs and their surrounding small clusters, were measured. Small clusters were separated from their nearest small neighbour by 0.2–3.1 μm (1.20 ± 0.45 μm, mean ± S.D.; $n = 1364$) and large discs were separated from their nearest large neighbour by 1.5–9.0 μm (mean of 4.16 ± 1.52 μm; $n = 139$). However, the distance from a large disc to its nearest 'small' neighbours was on average 2.4 ± 0.78 μm (range 0.2–5.0 μm; $n = 722$). Since this is about twice the normal spacing between small clusters, it implies that there is indeed a region of membrane surrounding each large disc that has a much lower incidence of immunoreactive punctae than would be expected in that area.

Kv2.1 channel immunolabelling and organization in interneurones

Since Kv2.1-IR is widespread in the ventral horn, it was of interest to determine if these channels are expressed by interneuronal populations as well as by α-motoneurones. Renshaw cells in ventral lamina VII can be easily identified by their gephyrin-IR (present at postsynaptic glycine/GABA synapses) and by calbindin d28K expression (see Alvarez *et al.* 1997; Carr *et al.* 1998). Dual immunolabelling demonstrated that Renshaw cells exhibit little or no Kv2.1-IR (Fig. 3*A*1). However, in the same sections as Kv2.1-negative Renshaw cells are observed, other calbindin-expressing interneurones in dorsal lamina VII (i.e. outside the Renshaw cell area) expressed strong membrane Kv2.1-IR (Fig. 3*A*2), suggesting that the paucity of Kv2.1-IR in Renshaw cells is not an artifact. The punctate somatic and dendritic membrane labelling of Kv2.1-IR interneurones was quite uniform in density and intensity, reflecting small–medium-sized clusters but lacking the large disc-like clusters of the type observed in α-motoneurones. Indeed, such large clusters were never seen in any other spinal neurones including dorsal spinocerebellar tract cells in Clarke's column.

Association of Kv2.1 clusters with synaptic inputs to α-motoneurones

Kv2.1-IR clusters in the surface (i.e. postsynaptic) membrane of motoneurones were invariably apposed by presynaptic terminals labelled with synaptophysin (Fig. 3*B*). The identity of the presynaptic terminals was investigated by using a variety of markers for serotoninergic (5-HT), glutamatergic, glycinergic/GABAergic, and cholinergic synapses. 5-HT terminals were seldom associated with postsynaptic Kv2.1-IR (Fig. 3*C*). Similarly, Kv2.1-IR was seldom seen colocalized with postsynaptic gephyrin-IR, suggesting that Kv2.1 channels are not present at glycinergic or GABAergic (inhibitory) synapses. Some glutamatergic (VGluT-1) terminals in apposition to motoneurones did associate with KV2.1-IR, primarily with small clusters (Fig. 3*D*). Dual labelling with VAChT, to label cholinergic terminals, revealed a striking correspondence between VAChT-IR presynaptic terminals and postsynaptic Kv2.1-IR (Fig. 4*A*). In particular, the VAChT-IR terminals were invariably associated with the large Kv2.1-IR clusters. Moreover, the VAChT-IR presynaptic terminals were clearly in the size range of the cholinergic C-terminals that uniquely innervate α-motoneurones (Alvarez *et al.* 1999; Wetts & Vaughn, 2001). High power images show the very close conjunction, with little or no overlap, of the respective fluorescence signals, strengthening the proposition that the observed Kv2.1-IR punctae are localized in the postsynaptic membrane (Fig. 4*A*, inset).

Muscarinic m2-type receptors are expressed by α-motoneurones and are concentrated postsynaptically below VAChT-IR C-terminal synapses (Skinner *et al.* 1999; Hellström *et al.* 2003). Therefore, we sought evidence for colocalization of m2-IR and Kv2.1-IR. The m2-IR

is prominent in the neuropil and around the somata of motoneurones in lamina IX (see also Welton *et al.* 1999). Somatic membrane domains of m2-IR clearly colocalize with large clusters of Kv2.1-IR (Fig. 4*B*). In this case, since the colocalized m2-IR and Kv2.1-IR are both in the postsynaptic membrane, there is complete overlap (yellow colour) of the two fluorescence signals (inset in Fig. 4*B*).

Ultrastructural observations

The confocal/fluorescence images and double labelling studies are highly suggestive that Kv2.1-IR punctae are localized to the postsynaptic membrane. Although the large disc-like Kv2.1 channel subunit-containing clusters are highly likely to be present at synaptic sites because of their clear and tight relationship to cholinergic terminals (and to the postsynaptically located m2 receptors), it is difficult to determine with immunofluorescence to what extent the much more numerous small clusters are associated with identifiable synapses. Pre-embedding peroxidase-based immunohistochemistry, with silver intensification, was therefore used to visualize Kv2.1-IR and its relationship to morphologically identified synapses on motoneurones.

The overall distribution of Kv2.1-IR was entirely consistent with the light microscopic observations in terms of its punctate nature and the size and separation of individual patches of immunoreactivity, although

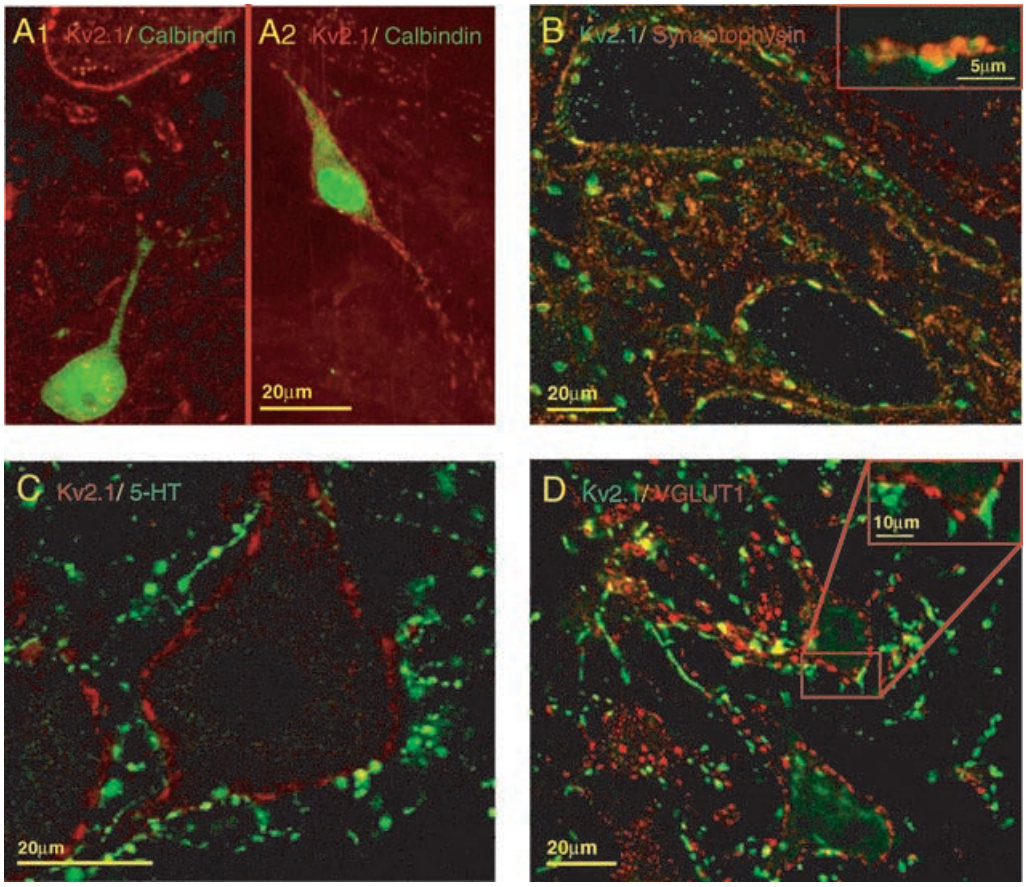

Figure 3.
A, Renshaw cell interneurones do not expresss Kv2.1. In *A*1, a Renshaw cell identified by calbindin expression (green cell at lower edge of image) is devoid of plasma membrane Kv2.1-IR, whereas the surface of a nearby motoneurone (seen at upper edge of image) displays typical intense Kv2.1-IR (red). In *A*2, a calbindin-IR interneurone outside the Renshaw cell area (located in dorso-medial lamina VII) expresses intense Kv2.1-IR. *B*, surface membrane Kv2.1-IR in motoneurones is apposed to presynaptic boutons labelled by synaptophysin. The inset shows a large synaptophysin-labelled terminal (red) very closely apposed to a large patch of surface membrane Kv2.1-IR (green). *C*, large discs of Kv2.1-IR (red) are not associated with 5-HT terminals (green) around the soma or proximal dendrites. *D*, some glutamatergic synaptic terminals are associated with postsynaptic Kv2.1-IR. VGluT1 terminals (green) are apposed to small patches of Kv2.1-IR (red; see inset for higher magnification)

some very small clusters detected by electron microscopy were likely below the limit of resolution of our light (confocal) microscopic techniques. Most importantly, all plasma membrane immunostaining appeared in the motoneurone, and not in presynaptic structures.

Quantitative ultrastructural analysis of the somatic region of 20 motoneurones (total length of membrane analysed, 4013 μm; total number of apposed boutons identified, $n = 369$) revealed S-type, F-type, and C-type terminals in the same relative frequency (33.6 $\pm$ 2.6%, 43.7 $\pm$ 2.5% and 16.9 $\pm$ 1.66%, respectively) and membrane coverage as in previous synaptological studies (see review by Fyffe, 2001). C-terminals are identifiable by electron microscopy by virtue of their large size and the presence of a subsynaptic cistern (see Introduction). In confirmation of the immunofluorescence data, every C-terminal observed in the electron microscope was associated with distinct Kv2.1-IR. Most importantly, the labelling was always concentrated at the postsynaptic side of the synaptic apposition, with very little migration of reaction product into the synaptic cleft (Fig. 5). The immunolabelling is concentrated close to the surface membrane, and appears closely associated with the subsynaptic cistern (Fig. 5*A*, *B* and *C*). The linear zone of labelling along a C-terminal/motoneurone apposition was somewhat discontinuous, but the immunoreactivity was distributed along almost the full length of the apposition. In single ultrathin sections the immunoreactive areas ranged from clusters of just a few gold particles to continuous bands over 1.5 μm long. Overall, on average, about 65% of the membrane postsynaptic to an individual C-terminal was immunolabelled.

Kv2.1-IR was also localized in association with other synaptic types, particularly the S-type synapse generally considered to be an excitatory synapse. Approximately 80% of somatic S-type synapses have postsynaptic Kv2.1-IR. Figure 5*E* shows one example, where there is a dense conglomeration of reaction product postsynaptic to an S-type bouton. An adjacent synapse is unlabelled. Again, the immunolabelling is clearly at the postsynaptic side of the synapse, and in some of these cases, the immunoreaction product is found extending up to 300 nm into the cytoplasm of the postsynaptic cell. It is likely that S-type synapses correlate with the VGluT1-labelled terminals seen in apposition to Kv2.1 clusters in the dual immunolabelling studies described above. Kv2.1-IR was not observed in association with F-type synapses (which are the most numerous type of synapse on the motoneurone soma), in agreement with the immunofluorescence data that showed little or no colocalization with gephyrin-IR (which is present at almost all F-type synapses on motoneurones).

Kv2.1-IR was observed in two other membrane-associated locations. First, there was a small amount of Kv2.1-IR associated with cytoplasmic membrane structures (Fig. 5*B* and *D*). These structures were typically close to zones of surface membrane labelling. On the other hand, the polyclonal (Alomone) antibodies used in some experiments produced more extensive cytoplasmic labelling, apparently localized in the endoplasmic reticulum and Golgi apparatus (not shown). Finally,

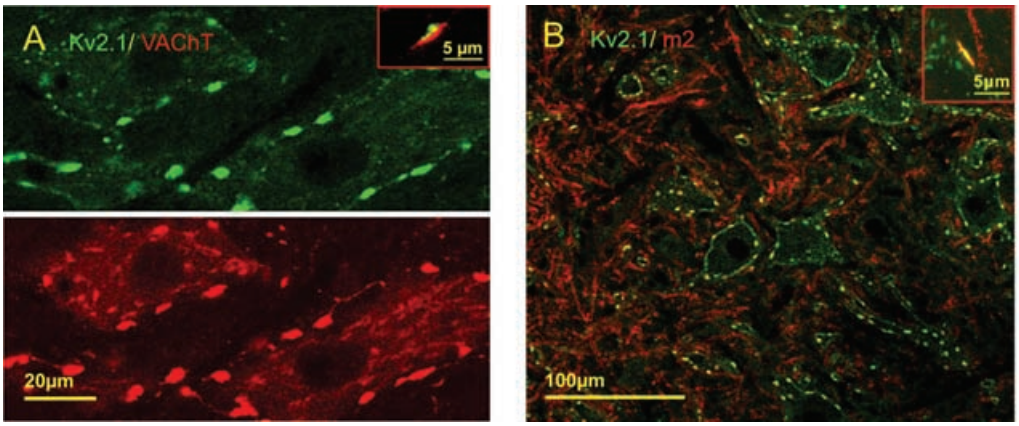

Figure 4.
Kv2.1 is specifically associated with large cholinergic terminals. *A*, a single optical section reveals precise spatial correspondence between VAChT-IR terminals (red) and surface membrane Kv2.1-IR (green). Every large VAChT-IR terminal is associated with a cluster of Kv2.1-IR. At low power, there appears to be some overlap (yellow) between the two channels, but at high power (inset) the red and green fluorescence signals are seen to be adjacent with minimal overlap. *B*, postsynaptic m2 muscarinic receptor (red) is colocalized with Kv2.1-IR (green). At low and high power (inset), the two channels of fluorescence signal overlap almost completely at the locations of large clusters of Kv2.1 (yellow, inset).

some patches of immunolabelling are associated with extrasynaptic surface membrane, apposed by presumed astrocytic processes (Fig. 5*D*). These extrasynaptic channel clusters varied in size up to about 0.5 μm in length and would be included in the population of small clusters seen with light microscopy.

Discussion

Membrane organization of Kv2.1 channels in spinal motoneurones

Complementary light and electron microscopic immunohistochemical localization of native Kv2.1 channel protein demonstrated the discontinuous or patchy distribution of these subunits in the plasma membrane. The relatively small amount of labelling within the cytoplasm appeared to be associated with intracellular membrane compartments, presumably involved in trafficking the channel protein to the cell surface membrane. Moreover, there was no evidence of a presynaptic localization of Kv2.1 at any synapses on motoneurones. As in other central neurones, Kv2.1 is thus expressed in a clustered distribution throughout the plasma membrane; however, there are significant differences in the subcellular distribution of Kv2.1 in spinal motoneurones compared with cortical or hippocampal neurones (see below).

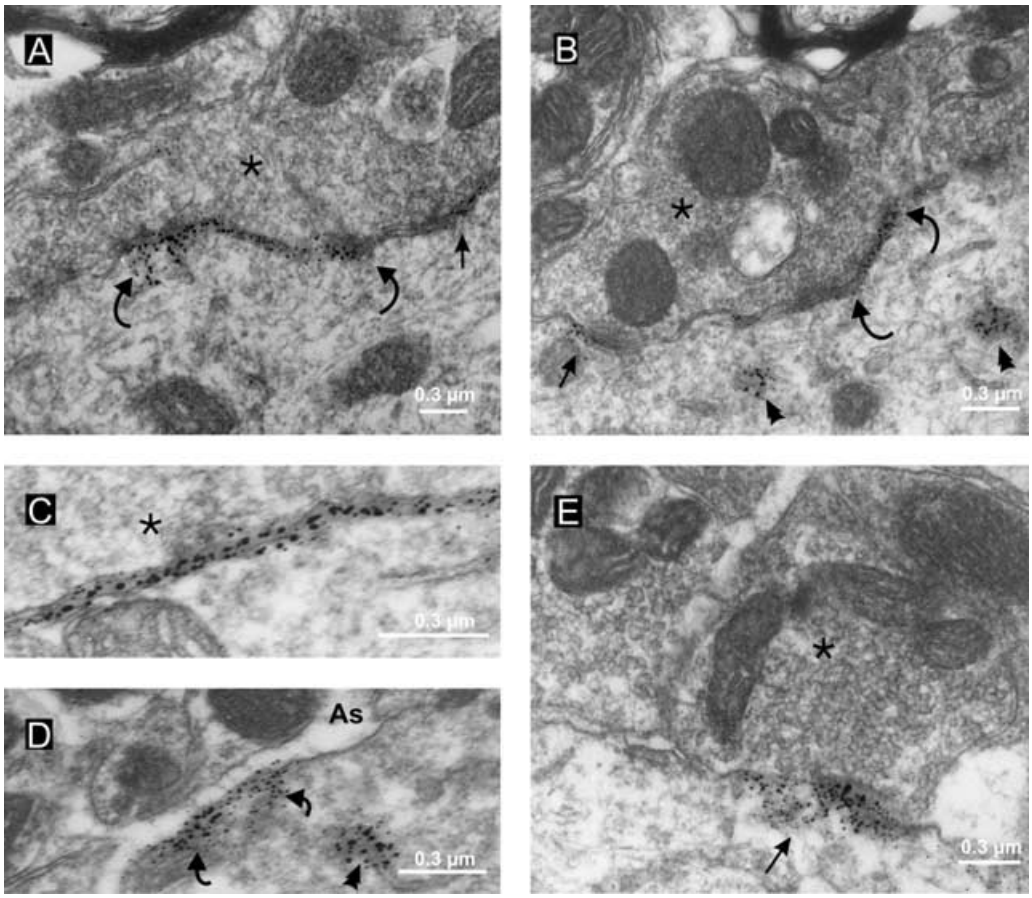

Figure 5.
Kv2.1-IR is restricted to the postsynaptic membrane and is clustered at specific synaptic sites on the membrane. Pre-embedding immunohistochemistry with silver intensification reveals Kv2.1-IR sites. *A* and *B*, small (arrows) and large (between curved arrows) regions of distinct membrane labelling are apposed to C-terminals (∗) on the motoneurone soma. The labelling is clearly postsynaptic, with rare particles of silver-intensified DAB reaction product apparently located (presumably because of diffusion of reaction product) in the synaptic cleft, and is associated with the subsurface cistern (*C*). *D*, occasional patches of extrasynaptic Kv2.1-IR are present in the plasma membrane apposed to finger-like astrocytic processes (As). Some cytoplasmic labelling is also visible in *B* and *D* (arrowheads), close to the regions of membrane labelling. *E*, intense postsynaptic Kv2.1-IR (arrow) at a synapse formed by an S-type terminal (∗); note that the membrane apposed to the adjacent terminal at left is unlabelled.

The mosaic of Kv2.1 subunit-containing channel clusters in motoneurones is comprised of highly variable sites, the majority of which are in the sub-micron range in extent. Notably, the clusters display about a 100-fold difference in area from the smallest to the largest clusters. The largest disc-like cluster aggregates cover areas of several square micrometres. The sensitivity and resolution of the imaging and measurement techniques, and our conservative criteria to avoid inclusion of small artifactual spots in the analysis, limits the ability of light microscopic analysis to detect (and measure) clusters smaller than about 0.1 μm^2. Based on our ultrastructural observations, it is possible that some surface membrane clusters are smaller than that limit. Nevertheless, the range of sizes measured with confocal microscopy probably gives a relatively accurate impression of the membrane domains harbouring Kv2.1 channel clusters.

In contrast to the broad range of punctae observed in motoneurones, Kv2.1-IR spinal interneurones and projection neurones express clusters of small to medium size distributed over their somatic surface membrane, and lack the large disc-like cluster aggregates that are prominent in motoneurones. Moreover, some spinal interneurones, including inhibitory Renshaw cells, express very low levels of Kv2.1, or even lack detectable levels of immunoreactivity altogether. Discrete surface membrane clusters of Kv2.1 channel subunits are also observed in principal neurones and interneurones throughout the central nervous system, as well as in cortical neurones in culture, where expression is highly polarized to the soma and most proximal dendrites (Scannevin *et al.* 1996; Du *et al.* 1998; Lim *et al.* 2000; Antonucci *et al.* 2001). On the other hand, the Kv2.1 subunit clustering in spinal motoneurones (and interneurones) is less spatially restricted since significant immunoreactivity is also detected in more distal dendritic membrane compartments. The existence of these cell type-specific expression patterns suggest that Kv2.1 targeting to clusters in the surface membrane relies on signals in addition to the intrinsic signalling domains of the channel protein (Lim *et al.* 2000), and might also be regulated by signals associated with other specific membrane components, and/or with specific synaptic inputs.

'*En face*' views of the cell surface obtained from high resolution confocal microscope images most effectively reveal the patchy mosaic of channel clusters in the surface membrane. The density of Kv2.1 clusters across the plasma membrane varies on a very small scale – even within the area of a large disc-like cluster there are microdomains of high or low channel density, because each disc is clearly comprised of many small, but discrete, punctae. Despite the large number of clusters per cell, we estimate that overall a rather small proportion, in the order of 10%, of the somatic membrane surface is enriched by Kv2.1 clusters. The clustered and patchy distribution could conceivably influence the frequency of detecting channels containing these subunits in recordings from membrane patches, especially since most of the clusters are localized under synapses. Interestingly, Safronov & Vogel (1996) noted that delayed rectifier channels were found at lower density than A-type channels in the somata of motoneurones, perhaps as a result of the specific distribution patterns described here.

The smallest punctae that we can detect presumably represent small clusters of single channels that have been targeted to the surface membrane, under intrinsic or extrinsic control (see above). It would therefore be of interest to determine if these small punctae represent the units from which larger and more complex clusters are formed. It is possible, for example, that the large disc-like structures which are surrounded by a halo of cluster-free membrane emerge as a result of lateral diffusion and aggregation of preformed small clusters into the large disc domain. However, the present results simply provide a snapshot of channel clustering, and additional studies are required to determine the dynamics and role of channel diffusion in the postsynaptic membrane (see Choquet & Triller, 2003).

Concentration of Kv2.1 immunoreactivity at somatic postsynaptic sites on motoneurones

The main finding of this study is that most of the Kv2.1 channel subunit protein is concentrated at specific postsynaptic sites on the soma and proximal dendrites. In particular, both confocal microscopy (dual labelling) and ultrastructural analysis confirmed that Kv2.1 expression is enriched at synapses formed by cholinergic C-terminals, and that the Kv2.1 subunit-containing channels are colocalized with postsynaptic m2 muscarinic receptors. Kv2.1-IR is also localized at a significant proportion of synapses formed by S-type, presumed excitatory, presynaptic boutons. The distribution of Kv2.1 at C- and S-type synapses contrasts with findings in hippocampal neurones, where Kv2.1 was selectively associated with symmetrical synapses (presumed inhibitory), and was particularly concentrated at extrasynaptic sites on the plasma membrane facing astrocytic processes (Du *et al.* 1998). In the present study, there was no association of Kv2.1 with inhibitory (F-type) synapses, and very little extrasynaptic clustering in proximity to astrocytic processes. These significant differences in subcellular

localization suggest that Kv2.1 channels subserve different roles in regulating excitability in different cell types.

In motoneurones, as in other central neurones, the global effect of Kv2.1 channel opening will be to decrease cell excitability. However, the presence of Kv2.1 at specific somatic synapses of diverse function raises the possibility that the modulation and/or role of the channel may be compartmentalized at the subcellular level. At S-type excitatory synapses, which are generally considered to operate via fast ionotropic receptor mechanisms, the opening of adjacent channels by a sufficiently large local synaptic depolarization would tend to limit the amplitude and/or time course of that synaptically induced depolarization. This modification of postsynaptic potentials would tend to counteract the increase in excitability that would otherwise occur, in keeping with the global role of these channels. However, at cholinergic C-type synapses, where there are extremely large clusters of channels, other mechanisms may come into play.

Neuronal M-currents are subserved by heteromeric KCNQ2 and KCNQ3 channels, and several lines of evidence implicate m1, rather than m2, receptors in the acetylcholine- (or muscarine-) induced suppression of these currents via a diffusible cytoplasmic second messenger (e.g. Hamilton *et al.* 1997; Marrion, 1997; Wang *et al.* 1998; Selyanko *et al.* 2000, 2001; Cooper *et al.* 2001). On the other hand, m2 receptors (which are unlikely to be involved in M-current modulation) appear to be the predominant muscarinic acetylcholine receptor (mAChR) type in the plasma membrane of motoneurones (Skinner *et al.* 1999; Welton *et al.* 1999; Rekling *et al.* 2000; Hellström *et al.* 2003; see also the present results). mAChRs m1–m5 transduce signals via distinct families of G proteins, and m2 activation can lead to sequential activation of various phosphorylation pathways (e.g. Hamilton *et al.* 1997; Marrion, 1997; Shapiro *et al.* 1999; Zhou *et al.* 2003; Tiran *et al.* 2003; Hoshi *et al.* 2003). Voltage-dependent activation of delayed rectifier Kv2.1 channels is markedly affected by phosphorylation, which shifts the activation curve of the channels to more positive membrane voltage levels (Murakoshi *et al.* 1997). Therefore, although there is evidence that acetylcholine (or muscarine) can alter motoneurone excitability via the M-current (e.g. Svirskis & Hounsgaard, 1998; Alaburda *et al.* 2002), it is possible that the striking juxtaposition of m2 receptors and Kv2.1 channels at cholinergic C-type synapses represents an opportunity for a novel mode of regulation involving these channels. The activation of m2 receptors by acetylcholine could result in a shift of the gating of the Kv2.1 potassium conductance into a range where the channels are not opened until more depolarized membrane potentials are reached (Murakoshi *et al.* 1997). This phosphorylation-mediated modulation of Kv2.1 would have the effect of increasing motoneurone excitability when C-terminals are activated. Although this mechanism is conceptually similar to that involving the M-current it clearly involves a different population of potassium channels and a different class of muscarinic receptor to the classic M-current.

Speculatively, modulation of the threshold of activation and $V_{\frac{1}{2}}$ values for Kv2.1 channels at C-terminal postsynaptic sites might be mediated, in a relatively 'fast' way, by direct binding of G protein $\beta\gamma$ dimers to the potassium channel, analogous to the inhibition of N- and P/Q-type calcium channels (Shapiro *et al.* 1999). Even when fully phosphorylated, Kv2.1 channels at C-synapses or elsewhere in the membrane could still be activated by large depolarizations, and could thus still play a role in action potential repolarization while playing a dynamic role in the regulation of excitability at the subthreshold level.

References

Alaburda A, Perrier JF & Hounsgaard J (2002). An M-like outward current regulates the excitability of spinal motoneurones in the adult turtle. *J Physiol* **540**, 875–881.

Alvarez FJ, Dewey DE, Harrington DA & Fyffe REW (1997). Cell-type specific organization of glycine receptor clusters in the mammalian spinal cord. *J Comp Neurol* **379**, 150–170.

Alvarez FJ, Dewey DE, McMillin P & Fyffe REW (1999). Distribution of cholinergic contacts on Renshaw cells in the rat spinal cord, a light microscopic study. *J Physiol* **515**, 787–797.

Antonucci DE, Lim ST, Vassanelli S & Trimmer JS (2001). Dynamic localization and clustering of dendritic Kv2.1 voltage-dependent potassium channels in developing hippocampal neurons. *Neuroscience* **108**, 69–81.

Bekkers JM (2000*a*). Properties of voltage-gated potassium currents in nucleated patches from large layer 5 cortical pyramidal neurons of the rat. *J Physiol* **525**, 593–609.

Bekkers JM (2000*b*). Distribution and activation of voltage-gated potassium channels in cell-attached and outside-out patches from large layer 5 cortical pyramidal neurons of the rat. *J Physiol* **525**, 611–620.

Blaine JT & Ribera AB (2001). Kv2 channels form delayed-rectifier potassium channels in situ. *J Neurosci* **21**, 1473–1480.

Brännström T (1993). Quantitative synaptology of functionally different types of cat medial gastrocnemius alpha-motoneurons. *J Comp Neurol* **330**, 439–454.

Carr PA, Alvarez FJ, Leman EA & Fyffe REW (1998). Calbindin D28k expression in immunohistochemically identified Renshaw cells. *Neuroreport* **9**, 2657–2661.

Chen XY & Wolpaw JR (1994). Triceps surae motoneuron morphology in the rat, a quantitative light microscopic study. *J Comp Neurol* **343**, 143–157.

Choquet D & Triller A (2003). The role of receptor diffusion in the organization of the postsynaptic membrane. *Nat Rev Neurosci* **4**, 251–265.

Conradi S (1969). Ultrastructure and distribution of neuronal and glial elements on the motoneuron surface in the lumbosacral spinal cord of the adult cat. *Acta Physiol Scand Suppl* **332**, 5–48.

Conradi S, Kellerth JO & Berthold CH (1979). Electron microscopic studies of serially sectioned cat spinal alpha-motoneurons. II. A method for the description of architecture and synaptology of the cell body and proximal dendritic segments. *J Comp Neurol* **184**, 741–754.

Cooper EC, Harrington E, Jan YN & Jan LY (2001). M channel KCNQ2 subunits are localized to key sites for control of neuronal network oscillations and synchronization in mouse brain. *J Neurosci* **21**, 9529–9540.

Du J, Tao-Cheng JH, Zerfas P & McBain CJ (1998). The K^+ channel, Kv2.1, is apposed to astrocytic processes and is associated with inhibitory postsynaptic membranes in hippocampal and cortical principal neurons and inhibitory interneurons. *Neuroscience* **84**, 37–48.

Fyffe REW (2001). Synaptic motoneurons, synaptic inputs and receptor organization. In *Motor Neurobiology of the Spinal Cord*, ed.Cope T, pp. 21–46. CRC Press, Boca Raton.

Fyffe REW, Ream LJ, Dewey R & Lujan R (2002). Differential distribution of Kv2.1 in spinal neurons. *FENS Abstr*. **1**, A216.4.

Gao BX & Ziskind-Conhaim L (1998). Development of ionic currents underlying changes in action potential waveforms in rat spinal motoneurons. *J Neurophysiol* **80**, 3047–3061.

Hamilton SE, Loose MD, Qi M, Levey AI, Hille B, McKnight GS, Idzerda RL & Nathanson NM (1997). Disruption of the m1 receptor gene ablates muscarinic receptor-dependent M current regulation and seizure activity in mice. *Proc Natl Acad Sci U S A* **94**, 13311–13316.

Hellström J, Arvidsson U, Elde R, Cullheim S & Meister B (1999). Differential expression of nerve terminal protein isoforms in VAChT-containing varicosities of the spinal cord ventral horn. *J Comp Neurol* **411**, 578–590.

Hellström J, Oliveira AL, Meister B & Cullheim S (2003). Large cholinergic nerve terminals on subsets of motoneurons and their relation to muscarinic receptor type 2. *J Comp Neurol* **460**, 476–486.

Hoffman DA, Magee JC, Colbert CM & Johnston D (1997). K^+ channel regulation of signal propagation in dendrites of hippocampal pyramidal neurons. *Nature* **387**, 869–875.

Hoshi N, Zhang JS, Omaki M, Takeuchi T, Yokoyama S, Wanaverbecq N, Langeberg LK, Yoneda Y, Scott JD, Brown DA & Higashida H (2003). AKAP150 signaling complex promotes suppression of the M-current by muscarinic agonists. *Nat Neurosci* **6**, 564–571.

Kellerth JO, Berthold CH & Conradi S (1979). Electron microscopic studies of serially sectioned cat spinal alpha-motoneurons. III. Motoneurons innervating fast-twitch (type FR) units of the gastrocnemius muscle. *J Comp Neurol* **184**, 755–767.

Kerschensteiner D, Monje F & Stocker M (2003). Structural determinants of the regulation of the voltage-gated potassium channel Kv2.1 by the modulatory α-subunit Kv9.3. *J Biol Chem* **278**, 18154–18161.

Kiehn O & Eken T (1998). Functional role of plateau potentials in vertebrate motor neurons. *Curr Opin Neurobiol* **8**, 746–752.

Kiehn O, Kjaerulff O, Tresch MC & Harris-Warrick RM (2000). Contributions of intrinsic motor neuron properties to the production of rhythmic motor output in the mammalian spinal cord. *Brain Res Bull* **53**, 649–659.

Korngreen A & Sakmann B (2000). Voltage-gated K^+ channels in layer 5 neocortical pyramidal neurones from young rats, subtypes and gradients. *J Physiol* **525**, 621–639.

Li W, Ochalski PA, Brimijoin S, Jordan LM & Nagy JI (1995). C-terminals on motoneurons, electron microscope localization of cholinergic markers in adult rats and antibody-induced depletion in neonates. *Neuroscience* **65**, 879–891.

Lim ST, Antonucci DE, Scannevin RH & Trimmer JS (2000). A novel targeting signal for proximal clustering of the Kv2.1 K^+ channel in hippocampal neurons. *Neuron* **25**, 385–397.

McLarnon JG (1995). Potassium currents in motoneurones. *Prog Neurobiol* **47**, 513–531.

Marrion NV (1997). Control of M-current. *Annu Rev Physiol* **59**, 483–504.

Muennich EAL, Ream LJ, Dewey DE & Fyffe REW (2002). Clustering of Kv2.1 potassium channels in spinal neurons. Program number 850.7, 2002 Abstract Viewer and Itinerary Planner. Society of Neuroscience, Washington, DC. http://sfn.scholarone.com

Murakoshi H, Shi G, Scannevin RH & Trimmer J (1997). Phosphorylation of the Kv2.1 K^+ channel alters voltage-dependent activation. *Mol Pharmacol* **52**, 821–828.

Murakoshi H & Trimmer JS (1999). Identification of the Kv2.1 K^+ channel as a major component of the delayed rectifier K^+ current in rat hippocampal neurons. *J Neurosci* **19**, 1728–1735.

Nagy JI, Yamamoto T & Jordan LM (1993). Evidence for the cholinergic nature of C-terminals associated with subsurface cisterns in alpha-motoneurons of rat. *Synapse* **15**, 17–32.

Powers RK & Binder MD (2001). Input-output functions of mammalian motoneurons. *Rev Physiol Biochem Pharmacol* **143**, 137–263.

Rekling JC, Funk GD, Bayliss DA, Dong XW & Feldman JL (2000). Synaptic control of motoneuronal excitability. *Physiol Rev* **80**, 767–852.

Ribera AB (1999). Potassium currents in developing neurons. *Ann N Y Acad Sci* **868**, 399–405.

Rose PK & Neuber-Hess M (1991). Morphology and frequency of axon terminals on the somata, proximal dendrites, and distal dendrites of dorsal neck motoneurons in the cat. *J Comp Neurol* **307**, 259–280.

Safronov BV, Bischoff U & Vogel W (1996). Single voltage-gated K^+ channels and their functions in small dorsal root ganglion neurones of rat. *J Physiol* **493**, 393–408.

Scannevin RH, Murakoshi H, Rhodes KJ & Trimmer JS (1996). Identification of a cytoplasmic domain important in the polarized expression and clustering of the Kv2.1 K^+ channel. *J Cell Biol* **135**, 1619–1632.

Selyanko AA, Hadley JK & Brown DA (2001). Properties of single M-type KCNQ2/KCNQ3 potassium channels expressed in mammalian cells. *J Physiol* **534**, 15–24.

Selyanko AA, Hadley JK, Wood IC, Abogadie FC, Jentsch TJ & Brown DA (2000). Inhibition of KCNQ1-4 potassium channels expressed in mammalian cells via M1 muscarinic acetylcholine receptors. *J Physiol* **522**, 349–355.

Shapiro MS, Loose MD, Hamilton SE, Nathanson NM, Gomeza J, Wess J & Hille B (1999). Assignment of muscarinic receptor subtypes mediating G-protein modulation of Ca^{2+} channels by using knockout mice. *Proc Natl Acad Sci U S A* **96**, 10899–10904.

Skinner JC, Alvarez FJ & Fyffe REW (1999). C-terminals are associated with postsynaptic muscarinic (M2) acetylcholine receptors in rat spinal cord alpha motoneurons. *Abstr Soc Neurosci* **25**, 1917.

Starr KA & Wolpaw JR (1994). Synaptic terminal coverage of primate triceps surae motoneurons. *J Comp Neurol* **345**, 345–358.

Storm JF (2000). K^+ channels and their distribution in large cortical pyramidal neurones. *J Physiol* **525**, 565–566.

Svirskis G & Hounsgaard J (1998). Transmitter regulation of plateau properties in turtle motoneurons. *J Neurophysiol* **79**, 45–50.

Takahashi T (1990). Membrane currents in visually identified motoneurones of neonatal rat spinal cord. *J Physiol* **423**, 27–46.

Tiran Z, Peretz A, Attali B & Elson A (2003). Phosphorylation-dependent regulation of Kv2.1 channel activity at tyrosine 124 by Src and by protein-tyrosine phosphatase epsilon. *J Biol Chem* **278**, 17509–17514.

Wang HS, Pan Z, Shi W, Brown BS, Wymore RS, Cohen IS, Dixon JE & McKinnon D (1998). KCNQ2 and KCNQ3 potassium channel subunits, molecular correlates of the M-channel. *Science* **282**, 1890–1893.

Welton J, Stewart W, Kerr R & Maxwell DJ (1999). Differential expression of the muscarinic m2 acetylcholine receptor by small and large motoneurons of the rat spinal cord. *Brain Res* **817**, 215–219.

Wetts R & Vaughn JE (2001). Development of cholinergic terminals around rat spinal motor neurons and their potential relationship to developmental cell death. *J Comp Neurol* **435**, 171–183.

Zhou H, Das S & Murthy KS (2003). Erk1/2- and p38 MAP kinase-dependent phosphorylation and activation of cPLA2 by m3 and m2 receptors. *Am J Physiol Gastrointest Liver Physiol* **284**, G472–G480.

Acknowledgements

We thank Dianne Dewey for outstanding assistance. This work was supported by NIH grant NS25547 to R.E.W.F.